PAPER

Check for updates

Ionizable lipid nanoparticles enhance lung delivery of gold nanoclusters for improving acute lung injury alleviation†

Yongning Bian,‡[a] Yanggege Li,‡[a] Dongfang Xia,[a] Yuanyu Huang,[b] Xueyun Gao, [ID] [a] Dongdong Su [ID] *[a] and Qing Yuan [ID] *[a]

Acute lung injury (ALI) is one of the most common and highly prevailing respiratory system diseases. However, there is still a lack of effective specialized medicines for the treatment of ALI. Biocompatible gold nanoclusters (AuNCs) have shown great potential in alleviating ALI, but their lung-targeted delivery needs to be enhanced. In recent years, lipid nanoparticles (LNPs) have become the most promising delivery system for clinical application and achieved great success in mRNA vaccines during the COVID-19 pandemic. Herein, we constructed a lung-delivery formulation of AuNCs by encapsulating glutathione-coated gold nanoclusters (GA) in lung-delivery ionizable lipid nanoparticles (iLNPs) and termed it as GA@iLNP. Results indicated that GA@iLNP can promote the cellular uptake of GA and enhance the anti-inflammation efficiency in stimulated macrophages *in vitro*. In addition, iLNP encapsulation significantly increased the lung accumulation of GA in lipopolysaccharide (LPS)-induced ALI mice after intravenous injection and enhanced the alleviations of inflammation and tissue damage in the lungs. These results suggest that organ-selective iLNPs may be an ideal targeted delivery system for AuNCs, providing a powerful tool for translational applications of bioactive AuNCs.

[a]*Center of Excellence for Environmental Safety and Biological Effects, Department of Chemistry, Beijing University of Technology, Beijing 100124, P. R. China. E-mail: chmsudd@bjut.edu.cn, yuanqing@bjut.edu.cn*
[b]*School of Life Science, Advanced Research Institute of Multidisciplinary Science, Beijing Institute of Technology, Beijing 100081, P. R. China*
†Electronic supplementary information (ESI) available. See DOI: https://doi.org/10.1039/d4nr05415f
‡These authors contributed equally to this work.

Qing Yuan received his PhD degree in Bioinorganic Chemistry from the University of Chinese Academy of Sciences (UCAS) in 2018. From 2011 to 2018, he worked as an Assistant Research Fellow at the Key Laboratory for Biomedical Effects of Nanomaterials and Nanosafety, CAS. He now works at Beijing University of Technology as an Associate Professor. His research interests focus on the biomedical applications and rational design and targeted delivery of bio-protected gold nanoclusters for the theranostics of malignant tumors and immune diseases.

Qing Yuan

1. Introduction

Acute lung injury (ALI) is a common respiratory system disease with high prevalence and one of the most common causes of mortality in critically ill patients.[1,2] ALI can be caused by a variety of endogenous and exogenous harmful factors, such as coronavirus infections, which have become a major public health concern.[3,4] There is still a lack of effective specialized medicines for the treatment of ALI, making it a major threat to global health and posing significant economic and social burdens.[1–4]

The pathogenesis of ALI is multifactorial, which involves complex immune and pathological processes that lead to lung dysfunction.[5] Immune dysregulation is a major driver of ALI; in particular, pro-inflammatory signalling plays a crucial role in aggravating lung injuries.[6,7] The excessive production of inflammatory cytokines rapidly causes ALI or the more severe acute respiratory syndrome (ARDS), resulting in increased permeability, pulmonary edema and respiratory distress, eventually leading to mortality.[8,9] Therefore, it is urgent to develop effective therapeutic methods to reduce the expression of inflammatory factors in injured lungs and alleviate ALI.[10]

In recent years, ultra-small gold nanoclusters (AuNCs) have emerged as one of the most promising nanomaterials in biomedical applications owing to their excellent biocompatibility,

unique physicochemical properties, and intrinsic biomedical activities.[11–15] In particular, their extensive inflammation-suppressing activity in immune cells and inflammatory disease models suggests their potential application in the treatment of ALI.[16–19] In a previous study, we demonstrated that gluta-thione-coated AuNCs (named GA) exhibited significant lung-protective activity in novel coronavirus disease 2019 (COVID-19)-infected transgenic mice and hamsters.[20] However, it was observed that in the infected animals, the amount of GA reaching the damaged lungs *via* intraperitoneal injection was much less than that *via* direct intranasal application.[20] Therefore, effective lung-targeting carriers are needed for GA to improve the efficiency of drug delivery to the lungs and reduce the systemic side effects of ALI treatment.

Recently, the success of mRNA vaccines during the COVID-19 pandemic has greatly highlighted the application promises of lipid nanoparticles (LNPs) as an *in vivo* delivery system.[21–23] LNPs have several advantages that make them ideal delivery vectors, including their simple preparation, high stability, high cell uptake efficiency, and strong endosomal escape ability.[24] Encouraged by the success of mRNA vaccines and the need for site-specific mRNA therapy, significant efforts have been dedicated to developing organ-selective LNPs for accumulating mRNA in specific organs.[24,25] Studies have shown that the targeting ability to different organs can be achieved by adjusting the proportion of lipids in LNP.[22] For example, adding a fifth ionizable lipid to the existing prescription of traditional four-component LNP and adjusting its proportion can achieve the selective targeting ability of different organs, including the liver, lung and spleen.[25,26] In addition to the targeted delivery of nucleic acid drugs, we speculate that loading AuNCs into organ-selective LNPs may have great potential to enable precise disease therapy (Scheme 1).

Herein, the therapeutic activity of GA in LPS-induced ALI mice was first determined by intratracheal administration. Then, a lung-delivery ionizable lipid nanoparticle (iLNP) was used for GA encapsulation and delivery, which was named GA@iLNP. The anti-inflammation activity of GA@iLNP was primarily verified in LPS-stimulated RAW264.7 cells *in vitro*. Next, the ALI alleviating activity and lung-delivery efficiency of GA@iLNP were evaluated in LPS-induced ALI mice *via* intravenous and intratracheal administration, respectively. Results indicated that GA@iLNP exhibits extraordinary stability and GA encapsulation efficiency. LNP encapsulation promotes the cellular uptake of GA in RAW264.7 cells, and results in more significant NF-κB pathway suppression and inflammatory inhibition in LPS-stimulated RAW264.7 cells. Intravenous administration of GA@iLNP significantly increased the distribution of GA in lung tissue and improved the therapeutic effects in LPS-induced ALI mice. In addition, GA@iLNP showed an obviously
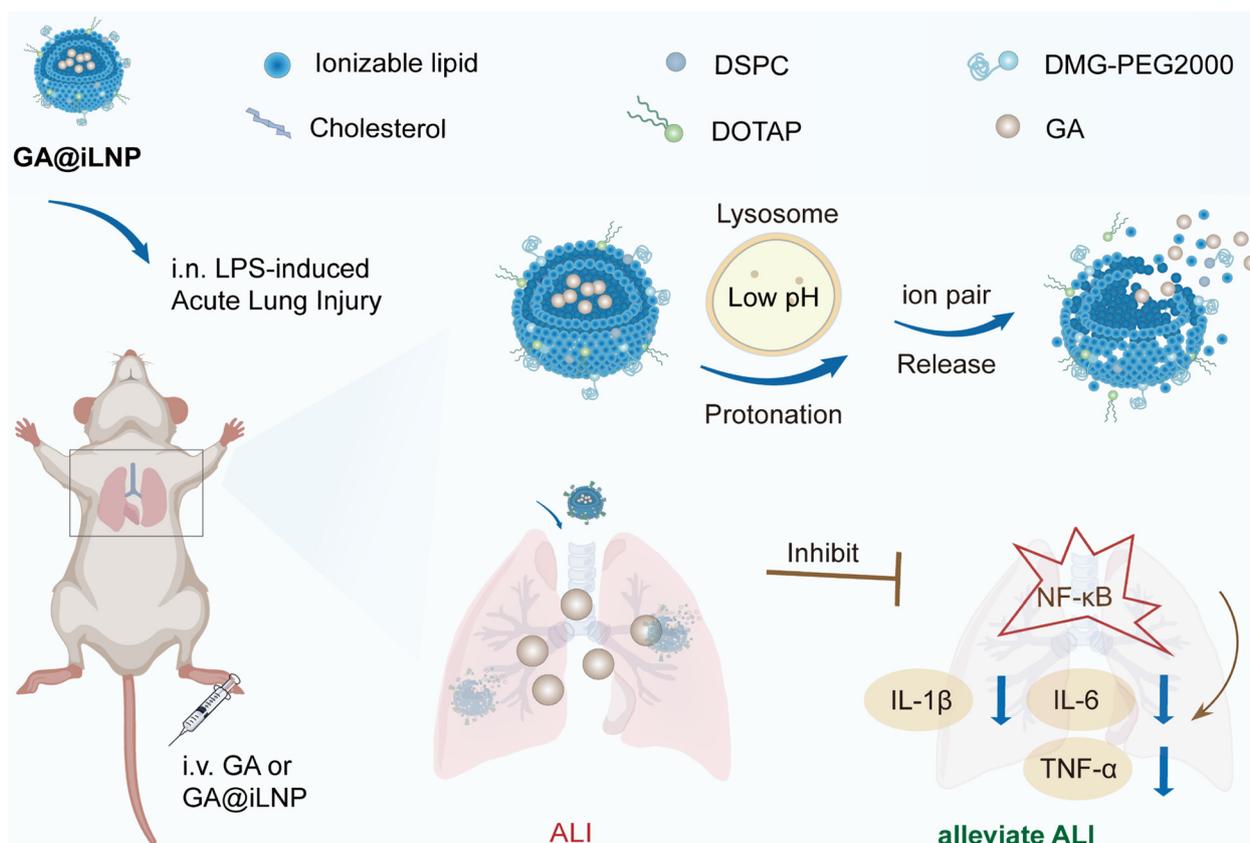
Scheme 1 Construction of GA@iLNP and the proposed lung-delivery and cellular release of GA in inflammatory lungs.

better therapeutic outcome for ALI than GA in inhalation therapy. These results highlight the great potential of organ-selective LNPs as suitable targeted delivery systems for AuNCs, expanding the application of LNPs beyond mRNA therapy, and provide a powerful tool for the translational applications of bioactive AuNCs.

2. Materials and methods

2.1. Materials and instrumentation

All chemicals and solvents were purchased commercially and used without further purification. Lipopolysaccharide (*Escherichia coli* O111:B4) was purchased from Sigma-Aldrich. $CySO_3^-$ was purchased from Xi'an Kaixin Biotechnology Co., Ltd. All cell culture media, fetal bovine serum (FBS) and phosphate buffered saline (PBS, pH 7.4) were purchased from HyClone. The ultrapure water (18 Ω) used in all experiments was obtained from the Milli-Q system (Millipore, USA). Spectroscopic data were measured on a FS5 Spectrofluorometer (Edinburgh Instruments Ltd, UK). Dynamic light scattering size and zeta potential were determined by a Malvern Mastersizer (Malvern Instruments Limited, England). The transmission electron microscopy images were recorded on a High-Resolution Transmission Electron Microscopy JEM-2100 (Japan Electronics Co., Ltd). The scanning transmission (STEM) images and energy spectrum (EDS) analysis were taken by field emission transmission electron microscopy (FEI Talos F200X-G2). The cytotoxicity of cells was recorded by the SpectraMax M4 Multi-Mode microplate reader. The qPCR was performed on a LightCycler96 real-time PCR system (Roche). The Au content of iLNP was analysed with High-Performance Liquid Chromatography-Inductively Coupled Plasma Mass Spectrometry (HPLC-ICP-MS) (Thermo-X7, USA). *In vivo* fluorescence images were obtained with an IVIS spectroscopy system (PerkinElmer, USA). The Micro Sprayer Aerosolizer (YAN-30012) was purchased from Shanghai Yuyan Instruments Co., Ltd.

2.2. Preparation of GA@iLNP

Ionizable lipids, 1,2-dioctadecanoyl-*sn-glycero*-3-phophocholine (DSPC), cholesterol, 1,2-dimyristoyl-*rac-glycero*-3-methoxypolyethylene glycol-2000 (DMG-PEG2000), and 1,2-dioleoyl-3-trimethylammonium-propane (DOTAP) were dissolved in 1 mL EtOH at a given molar ratio (Table S1†). The ionizable lipid was the same as that previously reported by our group.[27] Then, GA (32 mg mL^{-1}, 0.2 mL) was mixed with the above solution and rapidly added to the citrate buffer (3.6 mL, 0.05 M, pH 4.0) under stirring, and incubated for 10 min at room temperature. The formulations were dialyzed with 1× PBS overnight, and further concentrated using a 30 kDa ultrafiltration tube at 5000 rpm for 60 min.

2.3. Preparation of the fluorescent nanoprobe CySO$_3^-$@iLNP

The composition and proportion of lipid nanoparticles were the same as that described in the above section (Table S1†).

$CySO_3^-$ (20 mg mL^{-1}, 0.2 mL) was mixed with the above solution, and then added to citrate buffer (3.6 mL, 0.05 M, pH 4.0) under rapidly stirring, followed by incubation for 10 min at room temperature. The formulations were dialyzed with 1× PBS overnight.

2.4. Encapsulation efficiency

The encapsulation efficiency of GA@iLNP was investigated by quantifying the Au content in GA@iLNP. The data were provided by ICP-MS. After dialysis of the freshly prepared GA@iLNP with 1× PBS overnight, the sample underwent further ultrafiltration by a 30 kDa ultrafiltration tube to remove the free GA. The encapsulation efficiency was calculated *via* eqn (1):

$$\text{Encapsulation efficiency}\,(\%\,) = \frac{m\text{GA@iLNP}}{m\text{GA}} \times 100 \quad (1)$$

where mGA@iLNP is the Au content of GA@iLNP after ultrafiltration, and mGA is the total mass of the initial addition GA. The encapsulation efficiency loading capacity of GA in GA@iLNP was determined as 48.57%.

2.5. Cell culture

The RAW264.7 cell line was obtained from Cell Resource Centre, Peking Union Medical College. RAW264.7 cells were cultured in DMEM culture medium containing 10% (v/v) FBS and 1% (v/v) penicillin–streptomycin at 37 °C in a 5% CO$_2$ humidified atmosphere.

2.6. *In vitro* cytotoxicity assay

The cytotoxicity of GA@iLNP to RAW264.7 cells was measured by using standard Cell Counting Kit-8 system (CCK-8) assays. RAW264.7 cells were plated in a 96-well plate at 1×10^5 cells per well and incubated overnight in a cell incubator. After that, RAW264.7 cells were exposed to GA@iLNP at various concentrations for 24 h. After removing the supernatant, the CCK-8 reagent diluted with DMEM was added to each well and incubated for 1 h. Finally, the absorbance was measured at 450 nm by a microplate reader.

2.7. *In vitro* cellular uptake and inflammation suppression

The intracellular internalization ability of iLNP was verified at the cellular level. Macrophage RAW264.7 cells were incubated with GA and GA@iLNP (50 μM) for 4 h. Then, the cells were collected. After digestion, ICP-MS was used to quantify the intracellular Au content. Under different incubation conditions, the intracellular anti-inflammatory verification was measured. Four groups were then assigned, namely, control, LPS (1 μg mL^{-1}), LPS (1 μg mL^{-1}) + GA (50 μM), and LPS (1 μg mL^{-1}) + GA@iLNP (50 μM), and all groups were incubated for 24 h. Then, the total RNA of cells from each group was extracted to measure the mRNA expression of inflammatory factors by qPCR.

2.8. Animal and LPS-induced ALI

All animal procedures were conducted in accordance with the National guidelines of China, and approved by the Animal Ethics Committee of Beijing University of Technology (Approval No. HS202302002). BALB/c mice (about 18–20 g) were ordered from Beijing HFK Bioscience Co., Ltd, and fed water and food *ad libitum*. After the mice were anesthetized, a single intratracheal instillation of LPS at dose of 5 mg kg^{-1} was performed to induce acute lung injury.

## 2.9. *In vivo* distribution and lung accumulating ability

In vivo fluorescence imaging and *ex vivo* ICP-MS quantification were used to verify the distribution and lung aggregation of iLNP and GA. A fluorescence nanoprobe (CySO$_3^-$@iLNP, 100 μM, 100 μL) was intravenously injected, and *in vivo* fluorescence imaging was monitored at different time points (0, 0.5, 1, 2, 4, 6, 8 h). After 8 h, the mice were sacrificed and organs were harvested from each group, and the distribution of iLNP in different organs was observed. All mice were randomized, and the anti-inflammatory GA@iLNP (contained GA 5 mg kg^{-1}) was intravenously injected into the mice. The lungs were collected at 0, 0.5, 1, 2, 4 and 24 h after injection. Major organs were excised, weighed, and digested, and samples were prepared for testing after dilution in 1% HCl and 2% HNO$_3$. Finally, the Au content was determined by ICP-MS to quantify the distribution of GA in the lung and other organs.

2.10. *In vivo* ALI therapy study

The ALI model was established as described above. Mice were randomly divided into four groups: control group, LPS-induced ALI group, LPS + GA treatment group and LPS + GA@iLNP treatment group. The administration methods of the treatment group were divided into intratracheal instillation and intravenous injection. After the model was established, GA (5 mg kg^{-1}) and GA@iLNP (contained GA 5 mg kg^{-1}) were administered for anti-inflammatory treatment. Six hours after the last administration, the main organs were harvested, cut and digested to measure *via* ICP-MS to determine the organ distribution. In addition, the lung tissues were divided into several parts for Hematoxylin–eosin (HE) staining evaluation. The inflammatory cytokines were quantified by enzyme-linked immunosorbent assay (ELISA). The pathological score was assessed according to the overall degree of lung tissue injury (Fig. 1) or the detailed pathological injury items, including inflammatory infiltration, alveolar wall thickening, alveolar epithelial hyperplasia and hemorrhage (Fig. 4 and 5). Each subitem was graded from 0 to 4 (0 denotes no obvious abnormality, 1 denotes slight abnormality, 2 denotes mild abnormality, 3 denotes moderate abnormal, 4 denotes severe abnormality).

2.11. Statistical analyses

All data were expressed as mean ± SD. All statistical analyses were performed in Prism 9.3.1 (GraphPad) by unpaired Student's *t* test to analyse the differences between the two groups. A *P* value of less than 0.05 was considered to be statistically significant.
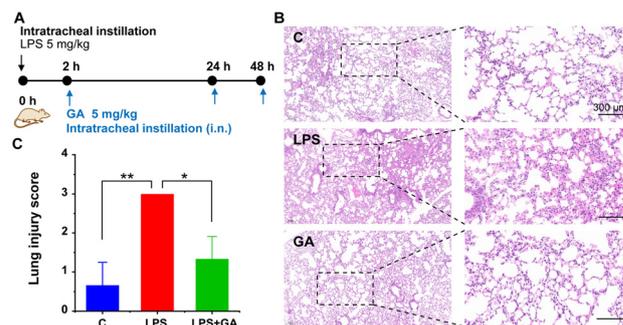
Fig. 1 (A) Schematic of the experimental procedure of GA treating LPS induced-ALI *via* intratracheal instillation in BALB/c mice. (B) Representative HE staining of lung tissue sections from each group. Scale bar, 300 μm. (C) Lung histopathological scores of each group; the method is overall score. Data are presented as mean ± SD, *n* = 5, *P* < 0.05, **P* < 0.01, compared with the LPS group.

3. Results and discussion

3.1. Alleviation activity of GA in LPS-induced ALI mice by inhalation therapy

The glutathione-coated gold nanocluster (GA) was prepared, as previously reported.[20] The hydrodynamic diameter of the obtained GA is approximately 1.80 nm with the PDI of 0.341, and analysed by dynamic laser scattering (DLS) (Fig. S1A†). Fluorescence spectra of GA showed that the excitation and emission peaks were 365 nm and 610 nm, respectively (Fig. S1B†). These characterization results are consistent with those previously reported.[16,20] Intratracheal instillation (*i.n.*) of LPS into BALB/c mice can cause significant ALI.[28] Thus, the effect of GA on alleviating ALI was evaluated in this LPS-induced ALI mice model (Fig. 1A). As shown in Fig. 1B, LPS induced obvious damage to the lungs, including pulmonary edema, inflammatory infiltration, alveolar epithelial hyperplasia and thickened alveolar septum, while GA treatment significantly alleviated these lesions. The results of the pathological score verified the therapeutic effects of GA on the LPS-induced ALI (Fig. 1C). However, we found a minimal distribution of GA in the mouse lungs after intravenous administration (Fig. S4†), which is consistent with previous reports.[29]

3.2. Preparation of the lung-delivery GA@iLNP

In order to enhance the bioavailability, GA was encapsulated with a lung-delivery iLNP to obtain GA@iLNP, which is expected to achieve a high GA accumulation in the lung with ALI. The preparation scheme of GA@iLNP is described in Fig. 2A. The lipid nanoparticle was composed of (ionizable lipid, cholesterol, DSPC, DMG-PEG2000) and GA with an optimized formulation, and GA@iLNP was constructed by a typical
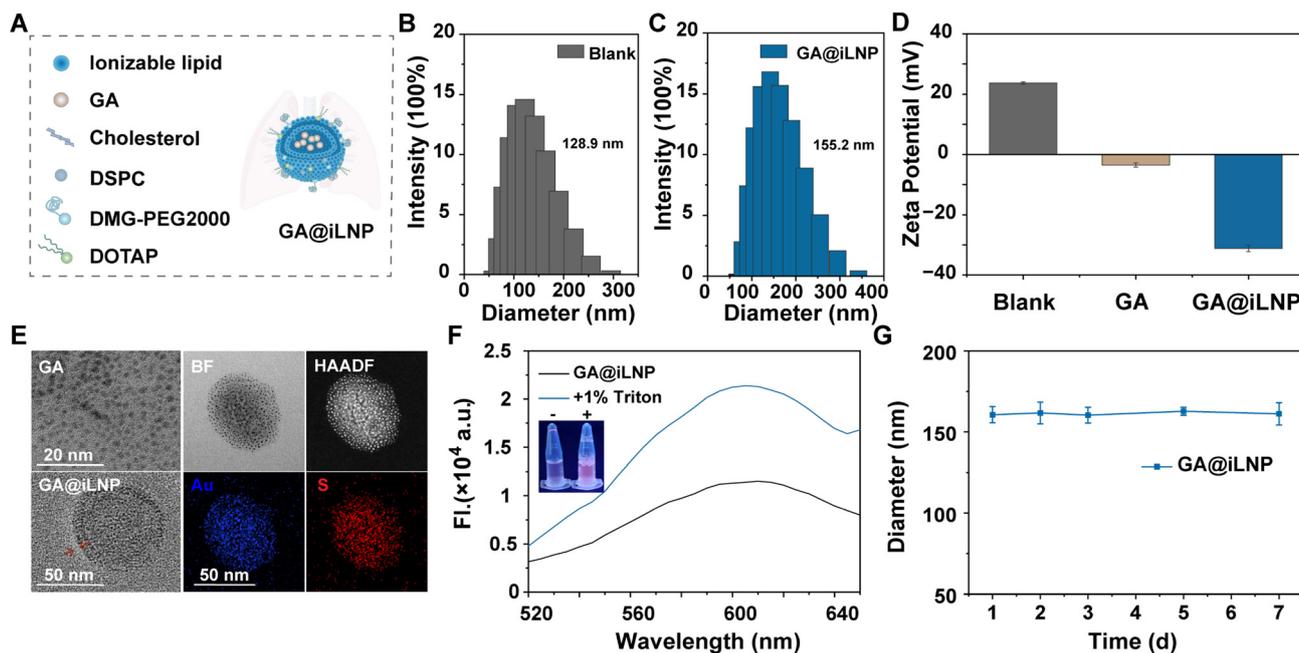
Fig. 2 Characterization of the physicochemical properties of GA@iLNP. (A) Composition and preparation of GA@iLNP. Hydrodynamic diameter distribution of blank lipids (B) and GA@iLNP (C). (D) Zeta potential of blank lipids, GA and GA@iLNP. (E) TEM images of GA and GA@iLNP, and STEM image combined with EDS elemental analysis of GA@iLNP. (F) Fluorescence spectra of GA@iLNP (50 μm) in the absence and presence of Triton X-100 (0.5%, v/v). (G) DLS sizes of GA@iLNP at different times after preparation.

solvent injection procedure (Table S1, and Fig. S2†). Firstly, the physicochemical properties of GA@iLNP were assessed, including the DLS size and zeta potential. The DLS size of the blank iLNP at a neutral pH was 128.9 nm with a PDI of 0.297, and the zeta potential was 23.7 mV, while the zeta potential of GA was −4 mV (Fig. 2B, D and S3A†). Due to the interaction between the positive and negative charges, GA with a negative charge can be effectively encapsulated by the positively charged iLNP theoretically. Indeed, after the formation of GA@iLNP, its diameter increased to 155.2 nm with the PDI of 0.136, and the zeta potential was −31.17 mV (Fig. 1C, D and S3A†). The morphological features of the proposed GA@iLNP were measured by transmission electron microscopy (TEM), which indicated that the size of the iLNP particles was 100.44 nm with a visible bilayer structure and internal monodisperse GA (Fig. 2E). Further elemental analysis on the GA@iLNP particle revealed that a large number of AuNCs were tightly confined within iLNP (Fig. 2E). These data demonstrated the successful construction of the GA@iLNP. Furthermore, after treatment with Triton X-100 to destroy the bilayer structure of GA@iLNP, a specific fluorescence signal of GA around 610 nm appeared (Fig. 2F). However, without the exogenous destroyer, the structure of GA@iLNP can be stable for at least 7 days (Fig. 2G and S3B†). The encapsulation efficiency of GA@iLNP determined by ICP-MS showed a high Au content at approximately 50%. These results confirmed that GA was successfully encapsulated by iLNPs, forming a pulmonary targeting nano-formulation GA@iLNP.

3.3. *In vitro* evaluating the anti-inflammation ability of GA@iLNP

To verify the anti-inflammatory ability of GA@iLNP, we used the macrophage cell line RAW264.7 as the *in vitro* model to mimic the inflammation development of ALI. Since GA showed excellent biocompatibility in previous studies, we further investigated the potential cytotoxicity of GA@iLNP to RAW264.7 cells. Different concentrations of GA@iLNP were incubated with RAW264.7 cells for 24 h, and the cell viability was tested by CCK8 assay. GA@iLNP did not induce any obvious cytotoxicity to RAW264.7 cells, even at doses of up to 200 μM (Fig. 3A). The cellular internalization of GA@iLNP may affect its anti-inflammatory ability. We compared the cellular uptake of GA and GA@iLNP in RAW264.7 cells at the same dose of 50 μM. After incubation for 24 h, the cells were collected to analyze the Au content in each group. ICP-MS quantification showed that, compared with the free GA, GA@iLNP significantly promoted the uptake by RAW264.7 cells (Fig. 3B).

Next, we explored the anti-inflammatory ability of GA@iLNP in LPS-stimulated RAW264.7 cells. Multiple proinflammatory cytokines, including interleukin-6 (IL-6), interleukin-1β (IL-1β) and tumor necrosis factor (TNF-α), are the main factors that affect lung inflammation in ALI.[8] To generate significant intracellular inflammation, RAW264.7 cells were stimulated with LPS (1 μg mL^{-1}) for 24 h, along with GA or GA@iLNP intervention. After treatment for 24 h, the total RNA of each group was extracted, and the mRNA expression of TNF-α, IL-1β and IL-6 was quantitatively analysed. As shown in
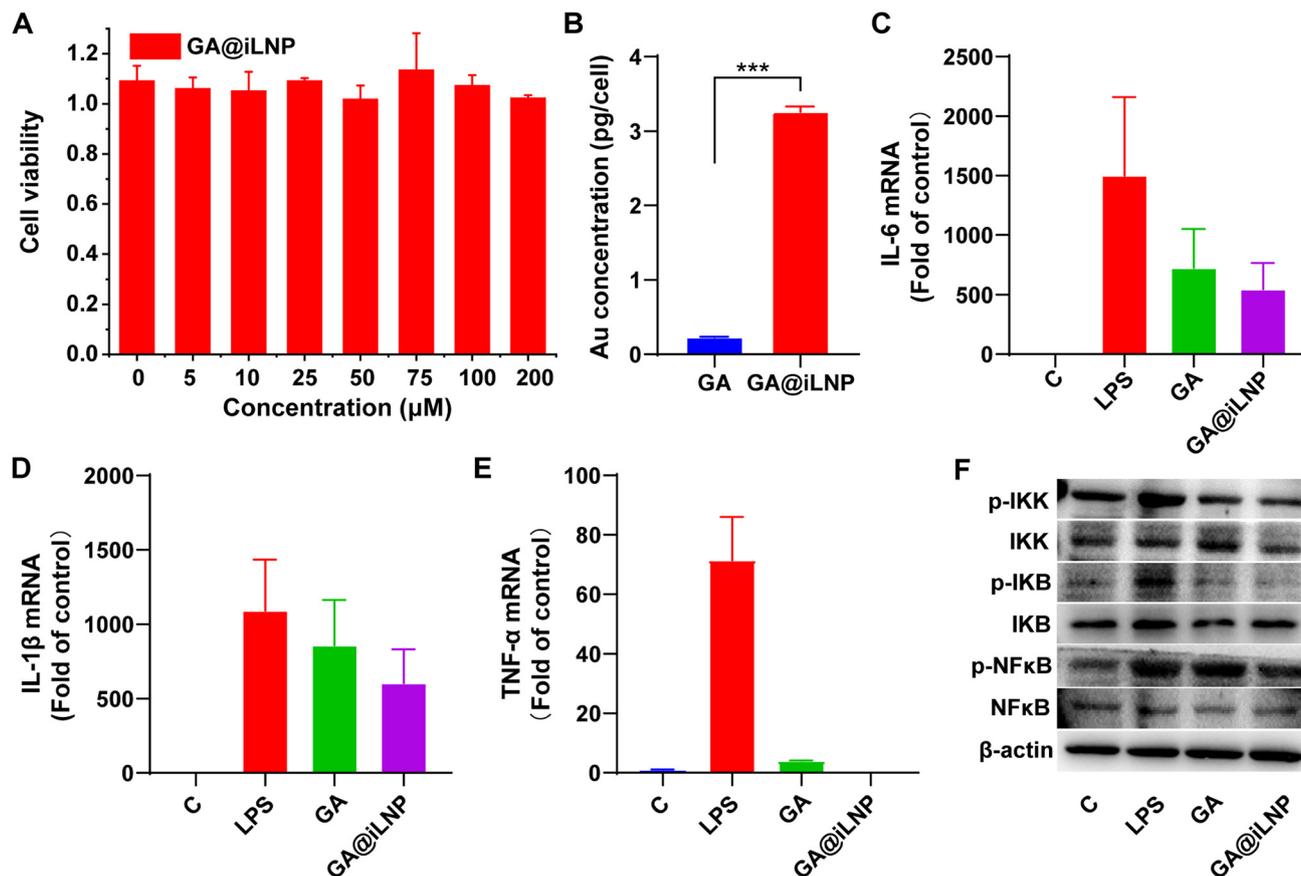
Fig. 3 Cellular uptake and anti-inflammation activity of GA@iLNP *in vitro*. (A) Cell viability of RAW264.7 cells after treatment with different concentrations of GA@iLNP. (B) Comparison of GA and GA@iLNP uptake by RAW264.7 cells. Data are presented as mean $\pm$ SD, $n = 3$, ***$P < 0.001$. The mRNA expression levels of IL-6 (C), IL-1β (D) and TNF-α (E) in different groups: control, LPS, LPS + GA. LPS + GA@iLNP, $n = 3$. (F) WB detection of the NF-κB signaling pathway in different groups.

Fig. 3C–E, LPS triggered significant expression of inflammatory cytokines, which were effectively down-regulated after treatment with GA and GA@iLNP. Compared with GA, GA@iLNP has a more significant inhibitory effect on TNF-α, IL-1β, and IL-6 expression, which is consistent with its better internalization in the cells. Nuclear factor-κB (NF-κB) is a major transcription factor that regulates the expression of these inflammatory cytokines.[10] We proposed that GA@iLNP could possibly suppress the expression of inflammatory factors through inhibiting the activation of the NF-κB signaling pathway. Western blotting (WB) detection showed that, compared with the LPS-stimulated group, the phosphorylation of IKK and its downstream I κB and NF-κB in the GA@iLNP-treated group were significantly reduced. This confirmed that GA@iLNP inhibited the activation of the NF-κB pathway, and was more effective than the same dose of GA (Fig. 3F). These results demonstrated that GA@iLNP showed enhanced cellular uptake and anti-inflammation ability *in vitro*.

3.4. *In vivo* evaluating therapeutic efficacy of GA@iLNP

To demonstrate the lung-accumulation of the iLNPs, we analysed its biodistribution *in vivo* after intravenous adminis-

tration (*i.v.*). Firstly, the fluorescent-labeled nanoprobes $CySO_3^-$@iLNP were intravenously injected into normal mice to acquire the *in vivo* fluorescence imaging at different time points (0, 0.5, 1, 2, 4, 6, 8 h) (Fig. S6A†). The fluorescent $CySO_3^-$ molecule has a sharp fluorescence emission at 800 nm, which is suitable for *in vivo* imaging due to its deep penetration (Fig. S5†). Results showed that the fluorescence of $CySO_3^-$@iLNP in the lung reached a peak before 4 h, and then gradually decreased over time (Fig. S6A†). After *i.v.* for 8 h, the main organs were isolated for *ex vivo* fluorescence imaging. Results indicated that the fluorescence signal was obviously distributed in the lung, except for accumulation in the liver (Fig. S6A†). The biodistribution of GA@iLNP in the lung of normal BALB/c mice over time was also detected by ICP-MS after intravenous injection. Quantitative analysis of the Au content by ICP-MS showed that GA@iLNP had the highest lung aggregation at 0.5 h and maintained high aggregation within 4 h, which was consistent with the fluorescence monitoring results (Fig. S6B†). In addition, we further compared the lung distribution between GA and GA@iLNP after a single dose of 5 mg kg^{-1} intravenous injection. The main organs were isolated after 6 h to analyse the

Au distribution by ICP mass spectrometry. Previous reports have shown that nontargeted GA is mainly distributed in the liver, spleen and kidney by biometabolism. However, there was considerable Au accumulation in the GA@iLNP-treated mouse lungs, and the amount was much higher than that in the unencapsulated GA-treated mouse lungs (Fig. S4†). Considering that GA@iLNP is also highly distributed in the liver and kidney, the potential biosafety was evaluated in a long-term treatment regimen in BALB/c mice. The mice were *i.v.* injected with GA@iLNP (5 mg kg^{-1}) every two days for two weeks, and the hematological changes were monitored on days 4, 8, and 12 (Fig. S7†). Results showed that the long-term treatment with GA@iLNP did not cause significant hematological changes (Table S2†) or abnormal liver function (ALT, AST and ALP) and kidney function (BUN and CREA), indicating an acceptable biosafety of GA@iLNP (Table S3†).

Based on the effective lung accumulation of GA@iLNP, we evaluated the therapeutic efficacy of GA@iLNP against LPS-induced ALI in BALB/c mice. The ALI model was established by *i.n.* administration with LPS (5 mg kg^{-1}), and then GA (5 mg kg^{-1}) or GA@iLNP (5 mg kg^{-1}) was *i.v.* injected after 2 h and 12 h for treatment (Fig. 4A). We found that GA@iLNP also has dramatic accumulation in the lungs under pathological conditions, and the overall bioavailability was greatly improved compared with GA, indicating that the results of the lung-delivery iLNPs were reproducible and may contribute to the

treatment of ALI (Fig. 4B). The pathological evaluation of lung tissues was assessed according to the International Harmonization of Nomenclature and Diagnostic Criteria (INHAND) scoring standard (Fig. 4C and D). The LPS-treated group showed the highest pathological injury, and the HE staining showed obvious alveolar epithelial hyperplasia and alveolar septal thickening, accompanied by neutrophil infiltration and partial bleeding (Fig. 4C). Treatment with GA or GA@iLNP significantly improved these pathological lesions. The average total pathological score of the GA-treated group was about 8.5, and that of the GA@iLNP-treated group was about 4, while the score for the untreated group exceeded 10 (Fig. 4D). Thus, the lung-delivery GA@iLNP showed more significant ALI alleviating activity than the non-targeted GA.

Next, we examined the levels of inflammatory factors in the lung tissues using ELISA. Compared with the LPS-stimulated group, the expressions of TNF-α, IL-1β and IL-6 in the lung tissue of the GA- and GA@iLNP-treated groups were significantly decreased, and GA@iLNP showed a more effective inhibitory effect (Fig. 4E–G). We also found significant weight loss in the LPS-induced ALI mice, and weight recovery after GA or GA@iLNP treatment (Fig. S8A†). These results indicated that intravenous administration of GA@iLNP can enhance the targeted delivery of more GA to the lungs, thus significantly suppressing inflammation and alleviating lung injuries. In
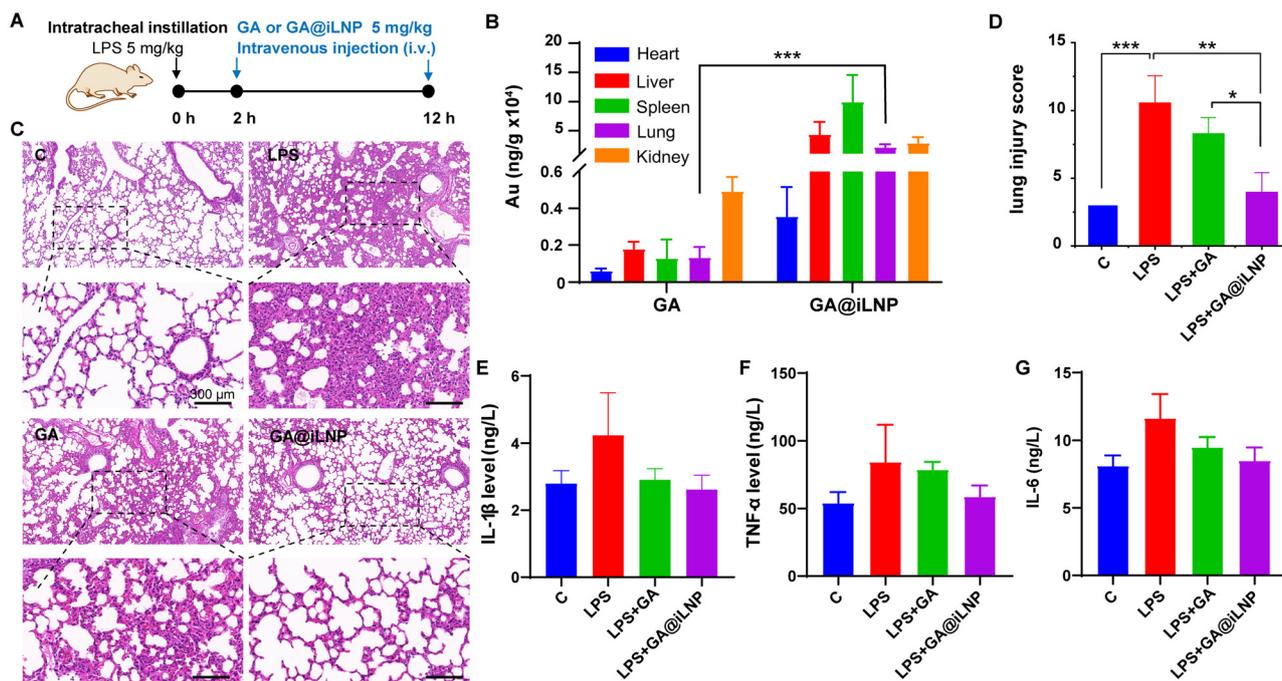
Fig. 4 (A) Schematic of the experimental procedure of GA and GA@iLNP treating LPS induced-ALI *via* intravenous administration in BALB/c mice. (B). Au distribution in major organs after treatment with GA or GA@iLNP. Data are presented as mean ± SD, *n* = 5. (C) Representative HE staining of the lung tissue sections from each group of control, LPS, LPS + GA, LPA + GA@iLNP. Data were assessed by scoring each subentry and performing statistical analysis of alveolar wall thickening, alveolar epithelial hyperplasia and inflammatory cell infiltration, and hemorrhage. *n* = 5, scale bar, 300 μm. (D) Histopathological scores of the lungs of each group. Data are presented as mean ± SD, *n* = 5, *P < 0.05, **P < 0.01, ***P < 0.001. The level of IL-1β (E), TNF-α (F) and IL-6 (G) in lung tissues was determined by ELISA detection, *n* = 5.
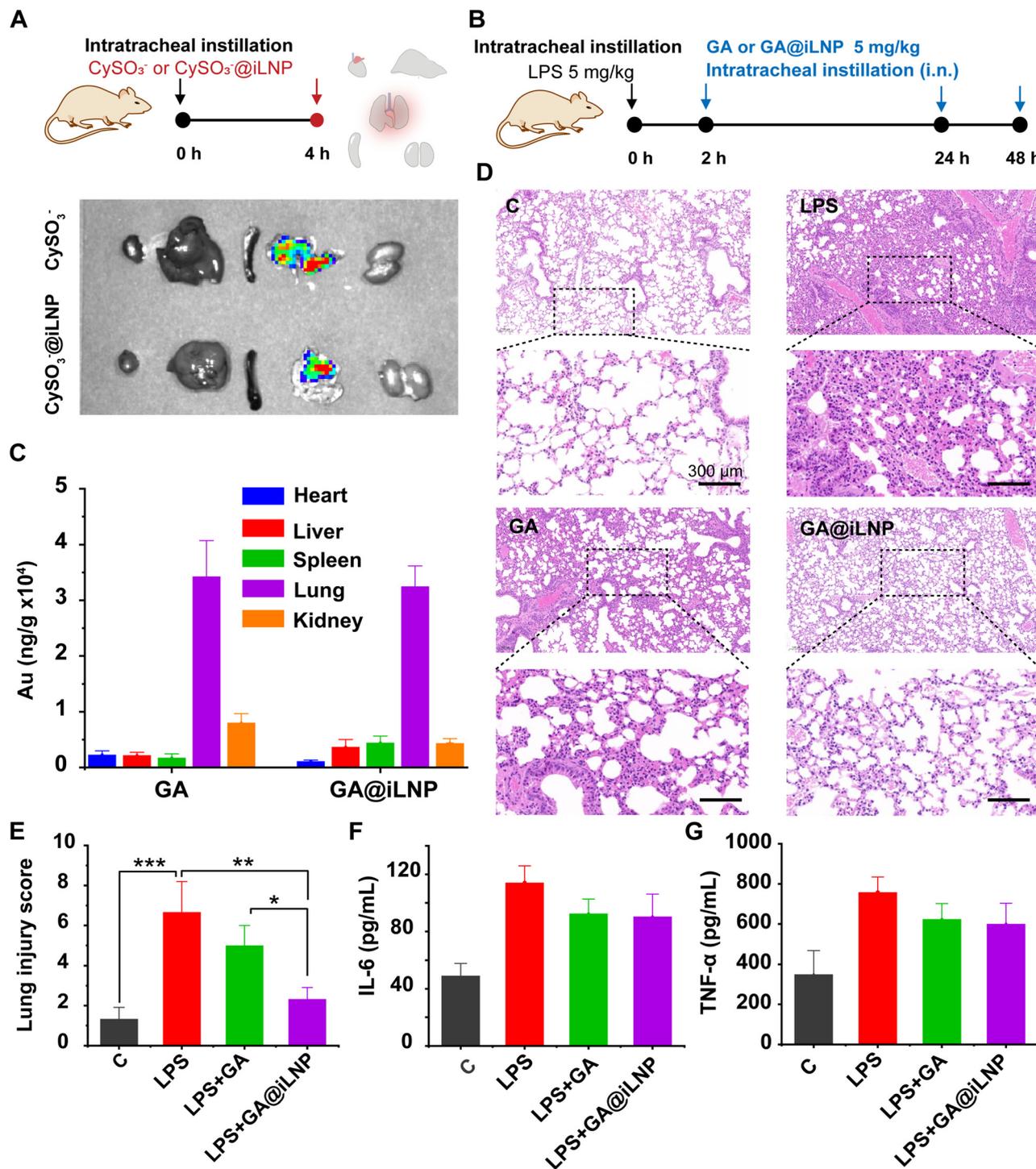
Fig. 5 (A) *Ex vivo* fluorescence imaging of $CySO_3^-$ and $CySO_3^-$@iLNP after intratracheal instillation in BALB/c mice. (B) Schematic of the experimental procedure of GA and GA@iLNP treating LPS induced-ALI *via* intratracheal instillation in BALB/c mice. (C) Au distribution in major organs. Data are presented as mean ± SD, n = 5. (D) Representative HE staining of lung tissue sections from each group. Scale bar, 300 μm. (E) Histopathological scores of the lungs of each group. Data were assessed by scoring each subentry and performing statistical analysis of alveolar wall thickening, alveolar epithelial hyperplasia, inflammatory cell infiltration, and hemorrhage. Data are presented as mean ± SD, n = 5, *P < 0.05, **P < 0.01, ***P < 0.001. The level of IL-6 (F) and TNF-α (G) in the lung tissues was determined by ELISA detection, n = 5.

addition, we collected other organs, including the heart, liver, spleen and kidney, from the GA@iLNP-treated mice and performed organ coefficient calculation and HE staining pathological analysis. The data showed that *i.v.* of GA@iLNP did not cause obvious damage to these organs (Fig. S8B and D†). We also evaluated the lung coefficients of normal mice that under-

went *i.v.* of GA or GA@iLNP. Results showed that the lung coefficients were the same as in the normal group, indicating they were safe for healthy lungs (Fig. S8C†). In short, GA@iLNP can effectively alleviate ALI and has good biosafety, showing its potential as a safe and reliable tool for ALI treatment.

3.5. *In vivo* evaluating intratracheal instillation therapy efficacy of GA@iLNP

Inhalation therapy is more amenable for patients than injection, and more conducive to clinical transformation.[30] Therefore, we further evaluated the ALI alleviating activity of GA@iLNP through intratracheal instillation (*i.n.*) administration. Firstly, we used the fluorescent probe $CySO_3^-$ to visually monitor the organ distribution of the iLNP after *i.n.* administration. The small molecular probe $CySO_3^-$ and nanoprobe $CySO_3^-$@iLNP were i.n. into the normal mice. After instillation of both probes for 4 h, the main organs were isolated to perform *ex vivo* fluorescence imaging. As shown in Fig. 5A, both fluorescent probes showed bright fluorescent signals in the lungs, indicating that *i.n.* can achieve more effective pulmonary delivery.

Based on the fluorescence imaging results, we treated the LPS-induced ALI BALB/c mice with GA or GA@iLNP by *i.n.* administration. The ALI model was still established by *i.n.* LPS (5 mg kg^{-1}), and the treated group was treated *via i.n.* GA (5 mg kg^{-1}) or GA@iLNP (content GA 5 mg kg^{-1}) for three times (2, 24 and 48 h after LPS-stimulation) (Fig. 5B). After treatment, the lung distribution of GA and pathological evaluation of the lung tissue, as well as the levels of proinflammatory cytokines in the lungs, were evaluated to determine the therapeutic effects. ICP-MS quantitative results showed that there was no significant difference in the Au accumulation in the lungs of ALI mice between the GA-treated group and GA@iLNP-treated group (Fig. 5C). As shown in Fig. 5D, the HE staining of the lung tissue sections showed that compared with normal mice, the LPS-induced ALI mice exhibited obvious alveolar wall thickening, alveolar stenosis, a large number of inflammatory infiltrations, and a small number of bronchioles and blood vessels congestion. GA and GA@iLNP treatment can both effectively reduce inflammatory infiltration and other lung injuries, while GA@iLNP showed better efficacy than GA. This observation was also confirmed by the pathological score (Fig. 5E). Then, the expression of inflammatory factors in the lung tissues was determined by ELISA detection, including TNF-α and IL-6. It was found that both GA and GA@iLNP treatment obviously reduced the elevated inflammatory cytokines in the lung tissue induced by LPS stimulation, but there was no significant difference in their inhibitory effects (Fig. 5F and G). However, GA@iLNP showed better improvement in the lung pathological evaluation. These results indicated that inhalation therapy with GA@iLNP in ALI also showed a better therapeutic outcome than unencapsulated GA.

4. Conclusions

Biocompatible glutathione-coated gold nanoclusters (GA) possess intrinsic anti-inflammatory activity, having previously exhibited lung-protection capability in COVID-19 infection-induced lung injury, but they lack lung-delivery capacity. This study aimed to enhance their lung-delivery, thereby increasing the therapeutic efficacy and reducing the systemic side effects in ALI treatment. Lipid nanoparticles (LNP) is one of the most promising delivery systems *in vivo*, and were approved in mRNA vaccines during the COVID-19 pandemic. Therefore, we encapsulated GA in a lung-delivery ionizable lipid nanoparticle (iLNP) to achieve lung-delivery in ALI alleviating treatment. Results demonstrated that the obtained formulation GA@iLNP improved the cellular uptake of GA in macrophage cells, and showed more significant activities on NF-κB pathway suppression and inflammatory factors inhibition. Notably, encapsulation with the iLNP significantly increased the distribution of GA in lung tissues of LPS-induced ALI mice, and improved the therapeutic effects with intravenous administration. In addition, GA@iLNP showed an obviously better therapeutic outcome for ALI than GA in inhalation therapy. These results indicated that organ-selective iLNP could be an effective delivery platform for bioactive AuNCs to achieve targeted delivery to specific sites *in vivo*, thereby improving the bioavailability of AuNCs and promoting their clinical applications.

Data availability

The data supporting this article have been included as part of the ESI.†

Conflicts of interest

The authors declare no conflict of interest.

Acknowledgements

References

1 M. A. Matthay, R. L. Zemans, G. A. Zimmerman, Y. M. Arabi, J. R. Beitler, A. Mercat, M. Herridge, A. G. Randolph and C. S. Calfee, *Nat. Rev. Dis. Primers*, 2019, **5**, 18.

2 M. B. Beasley, *Mod. Pathol.*, 2022, **35**, 1–7.

3 L. A. Mandell and M. S. Niederman, *N. Engl. J. Med.*, 2019, **380**, 651–663.

4 K. Kunzelmann, *Lancet Reg. Health Eur.*, 2021, **4**, 100094.

5 V. F. Corrales-Medina, D. M. Musher, S. Shachkina and J. A. Chirinos, *Lancet*, 2013, **381**, 496–505.

6 L. D. Bos and L. B. Ware, *Lancet*, 2022, **400**, 1145–1156.

7 Y. Imai, K. Kuba, G. G. Neely, R. Yaghubian-Malhami, T. Perkmann, G. van Loo, M. Ermolaeva, R. Veldhuizen, Y. C. Leung and H. Wang, *Cell*, 2008, **133**, 235–249.

8 P. Ward, *Eur. Respir. J.*, 2003, **22**, 22s–23s.

9 L. A. Huppert, M. A. Matthay and L. B. Ware, *Semin. Respir. Crit. Care Med.*, 2019, **40**, 31–39.

10 E. E. Abd El-Fattah, S. Saber, A. A. Mourad, E. El-Ahwany, N. A. Amin, S. Cavalu, G. Yahya, A. S. Saad, M. Alsharidah and A. Shata, *Biomed. Pharmacother.*, 2022, **147**, 112628.

11 G. Yang, Z. Wang, F. Du, F. Jiang, X. Yuan and J. Y. Ying, *J. Am. Chem. Soc.*, 2023, **145**, 11879–11898.

12 Q. Yuan, Y. Wang, L. Zhao, R. Liu, F. Gao, L. Gao and X. Gao, *Nanoscale*, 2016, **8**, 12095–12104.

13 C. Meng, Y. Liu, Y. Ming, C. Lu, Y. Li, Y. Zhang, D. Su, X. Gao and Q. Yuan, *Pharmaceutics*, 2024, **16**, 110.

14 D. Hao, X. Zhang, R. Su, Y. Wang and W. Qi, *J. Mater. Chem. B*, 2023, **11**, 5051–5070.

15 Q. Li, Y. Pan, T. Chen, Y. Du, H. Ge, B. Zhang, J. Xie, H. Yu and M. Zhu, *Nanoscale*, 2018, **10**, 10166–10172.

16 F. Gao, Q. Yuan, P. Cai, L. Gao, L. Zhao, M. Liu, Y. Yao, Z. Chai and X. Gao, *Adv. Sci.*, 2019, **6**, 1801671.

17 F. Gao, Q. Yuan, P. Cai, L. Gao, L. Zhao, M. Liu, Y. Yao, Z. Chai and X. Gao, *Adv. Sci.*, 2019, **6**, 1801671.

18 C. Lu, L. Xue, K. Luo, Y. Liu, J. Lai, X. Yao, Y. Xue, W. Huo, C. Meng and D. Xia, *ACS Nano*, 2023, **17**, 18421–18432.

19 H. Chen, Y. Jiang, T. Xu, J. Xu, J. Yu, Z. Chu, Y. Jiang, Y. Song, H. Wang and H. Qian, *J. Mater. Chem. B*, 2022, **10**, 4789–4799.

20 Z. He, F. Ye, C. Zhang, J. Fan, Z. Du, W. Zhao, Q. Yuan, W. Niu, F. Gao and B. He, *Nano Today*, 2022, **44**, 101468.

21 B. Li, R. S. Manan, S.-Q. Liang, A. Gordon, A. Jiang, A. Varley, G. Gao, R. Langer, W. Xue and D. Anderson, *Nat. Biotechnol.*, 2023, **41**, 1410–1415.

22 X. Xu and T. Xia, *ACS Nanosci. Au*, 2023, **3**, 192–203.

23 M. Baedeker, M. S. Ringel and U. Schulze, *Nat. Rev. Drug Discovery*, 2022, **21**, 90.

24 T. Zhang, H. Yin, Y. Li, H. Yang, K. Ge, J. Zhang, Q. Yuan, X. Dai, A. Naeem and Y. Weng, *Iscience*, 2024, **27**, 109804.

25 X. Wang, S. Liu, Y. Sun, X. Yu, S. M. Lee, Q. Cheng, T. Wei, J. Gong, J. Robinson and D. Zhang, *Nat. Protoc.*, 2023, **18**, 265–291.

26 Y. Bian, Y. Zhang, B. Hu, Y. Huang, W. Liang, Q. Yuan, J. Zhang, X. Gao and D. Su, *Small*, 2024, 2401282.

27 Y. Bian, Y. Zhang, B. Hu, Y. Huang, W. Liang, Q. Yuan, J. Zhang, X. Gao and D. Su, *Small*, 2024, **20**, e2401282.

28 R. J. Szarka, N. Wang, L. Gordon, P. Nation and R. H. Smith, *J. Immunol. Methods*, 1997, **202**, 49–57.

29 X.-D. Zhang, D. Wu, X. Shen, P.-X. Liu, F.-Y. Fan and S.-J. Fan, *Biomaterials*, 2012, **33**, 4628–4638.

30 C. Liu, L. Xi, Y. Liu, J. C. W. Mak, S. Mao, Z. Wang and Y. Zheng, *ACS Nano*, 2023, **17**, 11626–11644.